CONF-900623--23

PNL-SA--17555

DE91 005518

JAN 0 2 1991

MECHANICAL PROPERTY CHANGES AND MICROSTRUCTURES OF DISPERSION-STRENGTHENED COPPER ALLOYS AFTER NEUTRON IRRADIATION AT 411, 414, AND 529°C

K. R. Anderson[a]
F. A. Garner
M. L. Hamilton
J. F. Stubbins[a]

June 1990

For presentation at the 15th ASTM International Symposium of Effects of Radiation on Materials

Nashville, TN, June 17-21, 1990

Prepared for
the U.S. Department of Energy
under Contract DE-AC06-76RLO 1830

Pacific Northwest Laboratory
Richland, Washington 99352

(a) University of Illinois
Urbana, Illinois

DISCLAIMER

This report was prepared as an account of work sponsored by an agency of the United States Government. Neither the United States Government nor any agency thereof, nor any of their employees, makes any warranty, express or implied, or assumes any legal liability or responsibility for the accuracy, completeness, or usefulness of any information, apparatus, product, or process disclosed, or represents that its use would not infringe privately owned rights. Reference herein to any specific commercial product, process, or service by trade name, trademark, manufacturer, or otherwise does not necessarily constitute or imply its endorsement, recommendation, or favoring by the United States Government or any agency thereof. The views and opinions of authors expressed herein do not necessarily state or reflect those of the United States Government or any agency thereof.

MASTER

DISTRIBUTION OF THIS DOCUMENT IS UNLIMITED

MECHANICAL PROPERTY CHANGES AND MICROSTRUCTURES OF DISPERSION-STRENGTHENED COPPER ALLOYS AFTER NEUTRON IRRADIATION AT 411, 414, AND 529°C

Abstract

Dispersion strengthened copper alloys have shown promise for certain high heat flux applications in both near term and long term fusion devices. This study examines mechanical properties changes and microstructural evolution in several oxide dispersion strengthened alloys which were subjected to high levels of irradiation-induced displacement damage. Irradiations were carried out in FFTF to 34 and 50 dpa at 411-414°C and 32 dpa at 529°C.

The alloys include several oxide dispersion-strengthened alloys based on the Cu-Al system, as well as ones based on the Cu-Cr and Cu-Hf systems. Of this group, certain of the Cu-Al alloys, those produced by an internal oxidation technique to contain alumina weight fractions of 0.15 to 0.25% outperformed the other alloys in all respects. These alloys, designated CuAl15, CuAl20, and CuAl25, were found to be resistant to void swelling up to 50 dpa at 414°C, and to retain their superior mechanical and physical properties after extended irradiation. The major factor which controls the stability during irradiation was found to be the dispersoid volume fraction and distribution.

The other alloys examined were less resistant to radiation-induced properties changes for a variety of reasons. Some of these include dispersoid redistribution by ballistic resolution, effects of retained dissolved oxygen, and non-uniformity of dispersion distribution. The effect of laser welding was also

examined. This joining technique was found to be unacceptable since it destroys the dispersoid distribution and thereby the resistance of the alloys to radiation-induced damage.

Keywords: Copper alloys, dispersion strengthening, Cu-Al, Cu-Cr, Cu-Hf, mechanical properties, tensile properties, radiation damage, swelling, FFTF, welding.

MECHANICAL PROPERTY CHANGES AND MICROSTRUCTURES OF DISPERSION-STRENGTHENED COPPER ALLOYS AFTER NEUTRON IRRADIATION AT 411, 414, AND 529°C

Introduction

Severe radiation and thermal environments are foreseen in advanced nuclear reactor applications. These conditions require the development of new radiation resistant materials which are also immune to thermally induced problems, such as thermal shock, thermal fatigue, irradiation and thermal creep, and thermally induced static stresses. Many of these problems can be minimized by using high strength materials with high thermal conductivity. Copper-base alloys appear to fill this need. A significant number of scoping studies have identified one specific class of copper alloys as showing exceptional potential for use in these demanding nuclear applications: oxide-dispersed copper alloys.[1-16]

This study evaluates a wide variety of oxide-dispersed alloys and identifies the factors that influence their microstructure and mechanical property changes during irradiation. This evaluation, coupled with conductivity measurements, provides the basis for judging the suitability of specific oxide-dispersed alloys for fusion applications.

Experimental Procedure

Zone-refined, marz-grade copper and four different types of oxide-dispersed copper alloys were neutron irradiated in sealed helium-filled capsules in the Materials Open Test Assembly of the Fast Flux Test Facility to 34 displacements per atom (dpa) at 414°C, 50 dpa at 411°C, and 32 dpa at 529°C, Table 1. Irradiation temperatures were actively controlled to ±5°C. Two alloys were

irradiated in the laser-welded condition in order to determine the viability of this fabrication technique in nuclear service. Thermal aging was also performed at 420°C or 521°C for 1026 hours to assess alloy thermal stability.

The four types of oxide-dispersed alloys examined are shown, along with their composition and final processing condition, in Table 2. These alloys include three commercially available copper alloys strengthened by varying quantities of aluminum oxide (CuAl15, CuAl20, and CuAl25), one alloy strengthened by chromium oxide (CuCr), one alloy strengthened by hafnium oxide (CuHf), and two castable oxide-dispersed alloys. The grain sizes of these alloys prior to irradiation are provided in Table 3. More specific information regarding the sources and processing of these alloys is given elsewhere.[17] All specimens in this study were in the form of 3 mm TEM discs and miniature tensile specimens, the dimensions of which are given elsewhere.[18,19]

The tensile properties of unirradiated, thermally aged, and irradiated miniature tensile specimens were determined at room temperature using a precision horizontal tensile testing frame.[18] The 0.2% offset yield strength, ultimate tensile strength, fracture strength, uniform elongation, and total elongation were determined. Specimen thicknesses were measured with a micrometer prior to testing. All testing was performed at room temperature (24°C) at a crosshead velocity of 2.413×10^{-6} m/sec (9.5×10^{-5} in./sec), which corresponds to a strain rate of 4.7×10^{-4} sec^{-1}.

Fractography was performed with a JEOL JSM 35C scanning electron microscope (SEM). A JEOL 840 SEM with a Link Systems energy-dispersive x-ray spectros-

copy (EDS) and image analysis system was also used. Fracture surfaces required examination soon after tensile testing due to rapid formation of an oxide layer that obscured detail at magnifications over approximately 1000X. Examination of the bulk microstructure was carried out with a JEOL JEM 100CX transmission electron microscope (TEM) operated at 100 kV.

Results

The results of room temperature tensile tests are given in Table 4. The yield and ultimate tensile strengths generally showed the same behavior with respect to specimen condition. The trends in the yield and ultimate tensile strengths, and uniform and total elongations, are compared in Figure 1 for alloys irradiated at 411°C to 50 dpa. Data for marz Cu are included for comparison.

Tensile properties were sensitive to several types of microstructural changes during irradiation and, to a lesser extent, changes during thermal aging. The alloy dimensional stability under irradiation, primarily influenced by void swelling, is shown in Figure 2. That and other microstructural changes are discussed subsequently.

Discussion

The discussion of alloy performance is best grouped into four classes: copper-alumina alloys, the CuCr alloy, the CuHf alloy, and castable copper ODS alloys. It is clear, however, that the performance of all of these materials

is linked to dispersoid stability under irradiation and to the level of retained cold work.

Copper-Alumina Alloys

The three copper-alumina alloys in this study, CuAl15, CuAl20, and CuAl25, were produced using powder metallurgical, internal oxidation techniques by SCM Metal Products, Inc. under the trade name of Glidcop.[20] Their Universal Numbering System designations are C15715, C15720, and C15725. The alloys were produced from Cu powder containing small amounts of aluminum in solid solution. The powder was subjected to an elevated temperature oxidizing atmosphere where the aluminum was preferentially oxidized. The powder was then consolidated by rolling at elevated temperature between thin sheets of OFHC copper. The copper cladding, which served to reduce wear of the rolls and extrusion dies, was removed by sanding. The respective volume fractions of alumina in CuAl15, CuAl20, and CuAl25 are 0.7%, 1.0%, and 1.3%. Although the difference in alumina content is not the only variation between these alloys, it is by far the most important.

The aluminum oxide phase was determined by electron diffraction to be primarily gamma alumina, in agreement with the work of Livak et al.[10] Particle diameters ranged from 2 nm to 1 μm with an average of approximately 7 nm. This average particle size is close to the 12 nm particle size that provides maximum theoretical strengthening for alumina in copper.[21] Electron diffraction also revealed the presence of a significant quantity of Cu_2O in the

matrix, as would be expected from this alloy production technique. A trace quantity of alpha aluminum oxide and a relatively non-stoichiometric aluminum oxide were also observed in isolated regions of TEM foils. The oxide dispersions are not completely uniform; however the uniformity is the best available from commercial practice. The fine dispersion of gamma alumina not only serves to provide substantial Orowan strengthening, but also provides excellent retention of cold work at elevated temperature.[20]

The volumetric swelling of all three copper-alumina alloys was low, as shown in Figure 3. The swelling level was found to decrease with increasing volume fraction of alumina (Figure 4). While the three alloys had different levels of cold work, the amount of cold work has a minimal influence on swelling in these alloys. This was established from annealed, 20%, and 80% cold worked CuAl20 irradiated to 34 dpa at 414°C, which swelled -0.22, 0.31, and 0.30%, respectively.

A careful TEM through-focus series on several CuAl15, CuAl20, and CuAl25 specimens irradiated to 50 dpa revealed no void formation. However, in limited regions of foils where a low dispersoid density was present, a minimal yet distinct damage structure was observed. An example of this damage structure in CuAl15 irradiated to 50 dpa is shown in Figure 5. Frank loops ranging in size from 4.0 to 12 nm in diameter were present. A small quantity of helium bubbles measuring 3.2 to 20 nm in diameter with an average diameter of 4.0 nm were also seen. Both of these structures are often considered to be precursors to void formation. No neutron irradiation study has found void formation in copper-alumina alloys; however, a high damage level ion irradia-

tion study of CuAl60 by Spitznagel and Davis showed limited void formation in regions of low dispersoid density.[22] The helium bubbles are probably due to a ^{10}B (n,α) ^{7}Li thermal neutron reaction with the 200 ppm (max) boron remaining in this CuAl15 alloy following deoxidation.[23] If this is the case, the boron

must have been in solid solution rather than particulate form, since halos of helium and lithium, which form around boron-containing particles, were not observed.[24-27]

The room temperature tensile properties of these alloys in the unirradiated condition agree relatively well with those in the published industrial literature.[20] SEM fractography on broken tensile specimens, Figure 6, revealed the failure mechanism to be microvoid coalescence. Alumina particles of all sizes were observed to be sites for microvoid nucleation.

Room temperature tensile properties of these alloys following irradiation are dependent primarily on the amount of retained cold work. CuAl15, which was irradiated in the annealed condition, shows very small changes in the tensile properties following irradiation. However, recrystallization was observed following irradiation to 50 dpa at 411°C. Prior to irradiation, grains were elongated with an average grain size of 0.5 x 3.0 μm. Recrystallization during irradiation produced larger, more equiaxed grains measuring 1.4 x 2.5 μm on average. Despite recrystallization, significant decreases in Hall-Petch strengthening are not expected due to the small magnitude of this change and the decreased sensitivity of Hall-Petch strengthening at small grain sizes. In addition, the Hall-Petch strengthening for FCC metals is not as substantial as in BCC and HCP metals due to the larger number of slip systems and low critical stresses. The tensile failure morphology was microvoid coalescence, with fracture surfaces nearly identical in appearance to the fracture surfaces of unirradiated specimens, Figure 6.

The 20% cold worked CuAl20 exhibited significant reductions in strength and large increases in elongation for both the thermally aged and irradiated conditions. TEM examination of specimens irradiated to 50 dpa at 411°C revealed complete recovery and recrystallization. The average grain size prior to irradiation was 0.45 x 3.0 μm. Following irradiation to 50 dpa at 411°C, grains were equiaxed with an average grain diameter of 0.7 μm. The failure morphology of both unirradiated and irradiated miniature tensile specimens was by microvoid coalescence, though fewer large alumina particles were found on the irradiated alloy fracture surfaces, Figure 6. The only prior neutron irradiation studies of this alloy showed no significant mechanical property or microstructure changes following irradiation.[7-13] However those studies examined substantially lower damage levels, 3 and 15 dpa.

CuAl25 was irradiated in the 50% cold worked condition to 50 dpa at 411°C. TEM examination of irradiated specimens showed the alloy to be approximately 40% recrystallized. Prior to irradiation, this heavily cold worked alloy had an average grain size of 0.6 x 2.5 μm. During irradiation, recovery and recrystallization produced regions with equiaxed grains with 1.0 μm average diameter. Recrystallized areas contained a lower density of alumina particles than the unrecrystallized, slightly polygonized areas. These microstructural changes resulted in decreased strengths and increased elongations. However, the changes were not as large as in the fully recrystallized CuAl20 alloy. The tensile fracture surfaces, Figure 6, show a microvoid coalescence failure morphology. A decrease in the quantity of large alumina particles on the irradiated alloy fracture surfaces was observed, similar to CuAl20.

Previous neutron irradiation studies of CuAl25 involved tensile testing of specimens irradiated to 16 dpa at 430°C.[1-3] This work revealed decreased strengths and increased elongations in agreement with the results here. However, no recovery or recrystallization and only minimal microstructural changes were observed by TEM examination. It is possible that recovery and recrystallization may have been present, but not revealed by limited sampling volume during TEM examination.

There is substantial evidence for ballistic redistribution (recoil dissolution) of the alumina dispersion in these alloys by neutron irradiation. This evidence arises from three sources: immersion density measurements, SEM examination of fracture surfaces, and electron diffraction patterns. Neutron-induced recoil dissolution of particles, at its simplest, is a process where the atoms composing a particle are ballistically ejected by impinging neutrons.[27,28] Ballistic dissolution of the alumina dispersion was first considered after noting the densification of CuAl25 at 50 dpa. Commonly, densification is due to phase changes or phase modifications. In this simple, fully dense alloy, one change that could provide densification is dissolution of alumina. SEM fractography of CuAl20 and CuAl25 tensile specimens revealed a reduced quantity of large alumina particles following irradiation. (Only a very few large alumina particles were observed in the CuAl15 alloy prior to irradiation; therefore, no definitive statement can be made about dissolution in this alloy.) Densification may also arise from the formation of solid transmutants, primarily nickel and zinc. This possibility is being explored.

The best evidence for ballistic redistribution is taken from the electron diffraction patterns of CuAl20 and CuAl25 before and after irradiation. The characteristic ring patterns from the fine dispersion of particles in the unirradiated material decreased substantially in intensity following irradiation. In addition, the ring resolution became less distinct, suggesting radiation damage of the dispersoid itself. Figure 7 shows a larger alumina particle in CuAl15 for both the unirradiated and irradiated to 50 dpa at 411°C conditions, where a distinct damage structure in the irradiated alumina particle can be seen.

None of the previous neutron irradiation studies involving copper-alumina alloys have noted ballistic dissolution of the alumina dispersion. However, high energy ion irradiation of CuAl60 at 250 and 500°C to 20 dpa did cause dissolution and amorphization of the alumina particles.[22,28] Such recoil dissolution of particles has also been predicted theoretically.[29,30]

The dissolution phenomenon may have severe consequences. At higher damage levels, the alloy may become more susceptible to volumetric swelling by void formation due to both a decreasing amount of alumina and an increase in dissolved oxygen. This will also affect electrical and thermal conductivity. Furthermore, strength levels may suffer both due to the loss of particulate strength and the concomitant inability to retain cold work.

Laser welding was found to be an ineffective joining method for alumina-dispersed copper alloys. Laser butt welding of CuAl25 substantially reduced the quantity of alumina in the weld section. This loss of dispersion caused

irradiation-induced swelling and tensile property changes similar to those of marz copper.[19] The overall swelling of CuAl25 laser-welded TEM discs was approximately 9% due to void formation solely in the weld region. Unirradiated tensile strengths of welded specimens were slightly greater than for pure copper, but with nearly identical fracture surfaces. Following irradiation, similar results were found, however, the grain structure was columnar along the direction of welding and not equiaxed.

Copper-Chromium Oxide

The copper-chromium oxide alloy was produced by hot extrusion of a mixture of OFHC copper and chromium oxide powders. TEM and SEM examination revealed a range of chromium oxide particle sizes from 0.012 to 0.7 μm in diameter, with an average diameter of 0.05 μm. Electron diffraction also indicated the presence of a small quantity of Cu_2O in the matrix. Fractography of unirradiated tensile specimens revealed several large, irregularly shaped inclusions. The appearance and electrical charging of these inclusions during SEM examination suggests that they are ceramic. Windowless EDS chemical analysis showed varying quantities of calcium, magnesium, aluminum, and oxygen. These elements are the same as those commonly found in ceramic refractories, indicating that these inclusions were possibly pieces of ceramic furnace lining or slag in the original OFHC copper powder.

The volumetric swelling of this alloy was approximately 6% following irradiation to 50 dpa at 411°C, primarily due to void formation and dissolution of the refractory inclusions. SEM tensile fractography following irradiation

revealed both voids and the presence of other cavities containing only trace remnants of the refractory inclusions, Figure 8.

As in the case of the copper-alumina alloys, evidence of ballistic redistribution of the oxide dispersion was found. TEM examination of unirradiated material revealed large, relatively spherical chromium oxide particles, Figure 9. Following irradiation, these large particles were seen to be redistributed into smaller, less distinct particles with sizes ranging to below 2 nm in diameter, Figure 9. The redistribution of the oxide dispersion in this alloy is more prominent than in the copper-alumina alloys, probably due to the lower thermodynamic stability of chromium oxide compared to aluminum oxide.

Prior to irradiation, this alloy exhibited a moderate tensile strength and an elongation comparable to that of zone-refined copper. The failure morphology was transgranular by microvoid coalescence, Figure 8. The yield and ultimate strengths of this alloy changed only slightly following irradiation to 50 dpa at 411°C, even though TEM examination revealed substantial microstructural evolution. This is due to the competing influences of several strengthening mechanisms. The initial 20% cold work was completely recovered during irradiation. Recrystallization produced a grain size that was too large to be measured using TEM; high radioactivity precluded optical measurement. The reduction in cold work and grain size strengthening were offset by increased Orowan strengthening from a finer, redispersed particulate distribution and a slight contribution from voids, Figure 9.

The reduced total elongation in the irradiated alloy is a direct consequence of a limited reduction of area promoted by voids and cavities. Just as in zone-refined copper, voids acted as sites for failure by microvoid coalescence, reducing the ability of this alloy to undergo localized deformation. Cavities, which were previously occupied by inclusions, also acted as sites for crack nucleation and propagation, Figure 8.

Copper-Hafnium Oxide

The copper-hafnium oxide alloy was produced by a hot extrusion of a mixture of OFHC copper and hafnium oxide powders. SEM examination revealed large rounded hafnia particles ranging in diameter from 0.05 to 0.65 μm with an average of 0.25 μm. TEM bright and dark field imaging also revealed many smaller, less distinct hafnia particles, as small as 2.5 nm in diameter. A small quantity of Cu_2O was seen and many small unidentified particles also were manifested in the diffraction pattern as widely scattered spots.

Volumetric swelling of 0.15% was measured by density change following irradiation to 50 dpa. However, TEM examination found no signs of voids. Helium bubbles, Frank loops, and other precursors to void formation also were not observed.

TEM examination revealed extensive redistribution of the dispersion, again most probably by a ballistic mechanism. This was evidenced by a reduced quantity of the large, rounded hafnia particles as well as many smaller polygonal particles which were not present prior to irradiation. These

particles measured an average of 0.1 μm in diameter and are shown in Figure 10. A significant quantity of new particles, averaging 5 nm in diameter, of the same structure as the larger polygonal particles are also seen. SAD indicated that these particles are most probably monoclinic HfO_2.

This alloy exhibited good tensile strength and reasonable elongation in the unirradiated condition. The failure morphology was transgranular by microvoid coalescence, Figure 11. Thermal aging for 1026 hours at 420°C promoted a substantial reduction in tensile strength and increase in elongation, probably due to recovery of cold work.

The influence of the redistribution of the oxide dispersion was dramatically illustrated in the tensile properties of this alloy following irradiation to 50 dpa at 411°C. A prominent yield point drop was observed. This yield point phenomenon, commonplace in ferritic steels and other BCC metals, is highly unusual in FCC metals. Figure 12 shows tensile curves for this alloy in the unirradiated, thermally aged, and irradiated conditions. The irradiation-induced yield point is of approximately of the same magnitude as the ultimate tensile strength of this alloy. Following this yield drop, the tensile curve was wavy, becoming smoother at higher strains.

In addition to extensive redistribution of the oxide dispersion, TEM examination revealed total recovery and recrystallization during irradiation. Pinning of a low density of dislocations by redistributed hafnium is directly responsible for the unique tensile properties. There is some doubt as to the form of the redistributed hafnium. There is a large size difference (23%)

between copper and hafnium.[31] Thus, despite arguments for the lack of a shear component in the substitutional atom strain field and a consequent inability to pin screw dislocations, it may be that the large size difference would nevertheless cause such an effect here. Alternatively, dislocations may act as sites for preferential hafnium oxide reformation during irradiation, effectively pinning them with small hafnia particles. It was not possible to distinguish between these possibilities by TEM examination techniques.

Fractography revealed no apparent change of failure mechanism following irradiation. Failure was seen to occur by transgranular microvoid coalescence, Figure 11.

Castable ODS Copper Alloys

These alloys were cast from a melt composed of a fine dispersion of copper-coated colloidal oxide particles added to magnesium-bearing OFHC copper. Magnesium should promote effective incorporation and retention of the dispersed oxide during casting. One goal of the alloy design was to create a castable oxide-dispersed alloy that could also be welded.

These alloys showed extremely poor swelling resistance following irradiation to 50 dpa at 411°C: 10.75% for ODS-4 and 29.4% for ODS-1. The swelling level of ODS-1 was the same as pure copper under these irradiation conditions.

The unirradiated alloys exhibited minimal uniform tensile elongations due to microporosity, Figure 13. The microporosity was in the form of planar arrays

of bubbles along cold rolling directions. Laser-welded ODS-1 had spherical microporosity in the melted and undeformed weld region. Thermal aging at 420°C for 1026 hours promoted substantial decreases in strength and increases in elongations, verifying the poor thermal stability of these alloys.

Poor tensile properties following irradiation were due not only to poor thermal stability but also to substantial void formation. The failure morphology was identical to that observed in irradiated copper: transgranular by microvoid coalescence with surfaces often lying parallel to but not on the grain boundaries, Figure 13.[19]

The poor irradiation performance of these alloys is most probably attributable to a supersaturation of dissolved oxygen introduced during the casting process. However, it was not possible to obtain a measurement of the matrix oxygen concentration independent of the dispersed oxide to verify this postulate. Nevertheless, the microporosity found on fracture surfaces of unirradiated material supports this conclusion. Several researchers have shown that dissolved oxygen is highly efficient in promoting void formation in copper,[14-16,32] such as found here. Studies of electrolytic tough pitch copper irradiated in EBR-II to 13.5 dpa at 400°C found swelling of 34% or ~2.5%/dpa.[14-16] These results indicate that stringent oxygen-free casting practices must be observed when producing not only these alloys, but possibly other copper alloys. With such practice, it is possible that these castable ODS alloys would possess acceptable radiation resistance.

CONCLUSIONS

Zone-refined copper and several oxide-dispersed copper alloys were neutron irradiated to 34 dpa at 414°C, 50 dpa at 411°C, and 32 dpa at 529°C and a wide range of irradiation response was observed. The most important conclusions from this study are as follows:

1. The chemical composition of the dispersed oxide has a significant influence on the radiation resistance of oxide-dispersed alloys. Aluminum oxide-dispersed alloys were much more stable than either chromium or hafnium oxide-dispersed alloys. A highly unusual yield point phenomenon was observed in hafnium oxide-dispersed copper due to extensive redistribution of the oxide dispersion during irradiation.

2. All oxide-dispersed alloys showed some dissolution and restructuring of the dispersion by ballistic recoil during irradiation.

3. The radiation resistance of aluminum oxide-dispersed alloys (CuAl15, CuAl20, and CuAl25) was found to be directly dependent on the amount of dispersed oxide in the matrix. Volumetric swelling decreased as the amount of dispersed oxide increased, though it was small in all cases. No voids were found in these alloys.

4. The tensile properties of the aluminum oxide-dispersed alloys (CuAl15, CuAl20, and CuAl25) following irradiation were dependent on the amount of retained cold work, which was also related to the alumina content.

5. CuAl25 was found to be the most radiation-resistant alloy in terms of swelling, tensile properties, and conductivity.[32] It appears to be the best copper alloy for elevated temperature, neutron environment exposure.

6. Laser welding was found to be an ineffective joining method for oxide-dispersed alloys. A substantial loss of the dispersion in the weld region led to irradiation performance nearly identical to the poor performance observed in pure copper.

7. Oxygen contamination during casting must be prevented for copper alloys in nuclear service since oxygen promotes extensive radiation-induced void formation. Dissolved oxygen may become a concern even in the presence of oxide particles if ballistic dissolution places significant amounts of oxygen into solution.

REFERENCES

1. Brager, H. R., H. L. Heinisch, and F. A. Garner, J. Nucl. Mater. 133 & 134 (1985) 676-679.

2. Brager, H. R., J. Nucl. Mater. 141-143 (1986) 163-168.

3. Brager, H. R., J. Nucl. Mater. 141-143 (1986) 79-86.

4. Brager, H. R., and F. A. Garner, in Fusion Reactor Materials, DOE/ER-0313/3 (1987), 254-259.

5. Brager, H. R., and F. A. Garner, in Effects of Radiation on Materials: 14th International Symposium (Volume II), ASTM STP 1046, N. H. Packan, R. E. Stoller and A. S. Kumar, eds., American Society for Testing an Materials (1990), pp. 599-604.

6. Garner, F. A., H. R. Brager and K. R. Anderson, "Neutron-Induced Changes in Density and Electrical Conductivity of Copper Alloys at 16 to 98 dpa and 430°C," to be published in J. Nucl. Mater. 176 (1990).

7. Livak, R. J., T. G. Zocco, and J. C. Kennedy, in ADIP Semiannual Progress Report, DOE/ER-0045/14 (1985), 152-160.

8. Frost, H. M., and J. C. Kennedy, in ADIP Semiannual Progress Report, DOE/ER-0045/14 (1985), 161-167.

9. Livak, R. J., L. S. Leinson, and E. K. Opperman, Trans. ANS 49 (1985) 106.

10. Livak, R. J., T. G. Zocco, and L. W. Hobbs, in Damage Analysis and Fundamental Studies, DOE/ER-0046/24 (1986), 94-99.

11. Livak, R. J., H. M. Frost, T. G. Zocco, J. C. Kennedy, and L. W. Hobbs, J. Nucl. Mater. 141-143 (1986) 160-162.

12. Frost, H. M., and J. C. Kennedy, J. Nucl. Mater. 141-143 (1986) 169-173.

13. Livak, R. J., T. G. Zocco, and L. W. Hobbs, J. Nucl. Mater. 144 (1987) 121-127.

14. Ames, M., G. Kohse, T. S. Lee, N. J. Grant, and O. K. Harling, J. Nucl. Mater. 141-143 (1986) 174-178.

15. Lee, T. S., L. W. Hobbs, G. Kohse, M. Ames, O. K. Harling, and N. J. Grant, J. Nucl. Mater. 141-143 (1986) 179-183.

16. Harling, O. K., N. J. Grant, G. Kohse, M. Ames, T-S Lee, and L. W. Hobbs, J. Mater. Res. 2(5) (1987) 568-579.

17. Anderson, K. R., PhD Thesis, University of Illinois at Urbana-Champaign, Department of Materials Science and Engineering (1990).

18. Panayotou, N. F., S. D. Atkin, R. J. Puigh, and B. A. Chin, "Design and Use of Nonstandard Tensile Specimens for Irradiated Materials Testing," in The Use of Small-Scale Specimens for Testing Irradiated Materials, ASTM STP 888 (1986), 201-219.

19. Anderson, K. R., F. A. Garner, and J. F. Stubbins, "Unusual Tensile and Fracture Behavior of Pure Copper at High Levels of Neutron-Induced Swelling," this conference.

20. Glidcop, SCM Metal Products, Inc., 11000 Cedar Avenue, Cleveland, Ohio 44016, U.S.A. (1988).

21. Kupcis, O. A., B. Ramaswami, and O. T. Woo, Acta Met 21 (1973) 1131.

22. Spitznagel, J. A., and J. W. Davis, in ADIP Semiannual Progress Report, DOE/ER-0045/14 (1985), 168.

23. Zinkle, S. J., in Fusion Reactor Materials, DOE/ER-0313/6 (1989).

24. Hishinuma, A., Y. Katano, and K. Shiraishi, J. Nucl. Mater. 52 (1974) 103-111.

25. Gelles, D. S., and F. A. Garner, J. Nucl. Mater. 85-86 (1979) 689.

26. Vela, P., J. Hardy, and B. Russel, J. Nucl. Mater. 26 (1968) 129.

27. Kumar, A. S., and F. A. Garner, Rad. Effects 82 (1984) 61-72.

28. Spitznagel, J. A., N. J. Doyle, W. J. Choyke, J. G. Greggi, Jr., J. N. McGruer, and J. W. Davis, Nucl. Instr. and Meth. in Phys. Res. B16 (1986) 279-287.

29. Frost, H. J., and K. C. Russell, Acta Met. 30 (1982) 953-960.

30. Russell, K. C., Progress in Mat. Sci. 28 (1984) 229-434.

31. Wert, C. A., and R. M. Thomson, Physics of Solids, Second Edition, McGraw-Hill, New York, 1970, p. 23.

32. F. A. Garner, K. R. Anderson and T. Shikama, "Radiation-Induced Changes in Electrical Conductivity of a Wide Range of Copper Alloys, presented at this conference.

TABLE 1

Specimen Irradiation Conditions

Alloy	Material Code	MOTA IE 411°C 50 dpa	MOTA ID 414°C 34 dpa	MOTA ID 529°C[a] 32 dpa
Marz Cu	RO	d/t[b]	d/t	d[c]
CuAl25	R4	d/t	--	--
CuAl25 (welded)	3N	d/t	--	--
CuAl20	UX	d/t	d/t	d/t
CuAl15 +B	VO	d	d/t	d
ODS-1	3F	d/t	-	--
ODS-1 (welded)	3H	d/t	--	--
ODS-4	3M	d/t	--	--
CuCr	3A	d/t	--	--
CuHf	3B	d/t	--	--

(a) Overtemperature of 201°C for 50 minutes and 2 undertemperatures.
(b) d/t = TEM discs + tensiles.
(c) d = TEM discs.

TABLE 2

Composition and Final Processing Conditions of Copper Alloys

Alloy	Code	Composition (wt%)	Final Processing Condition[a][b]
Marz Cu	RO	99.999% Cu	Annealed
CuAl25	R4	0.25% Al as Alumina, bal. Cu	50% CW
CuAl25	3N	0.25% Al as Alumina, bal. Cu	50% CW + welded
CuAl20	UX	0.20% Al as Alumina, bal. Cu	20% CW
CuAl15+B	VO	0.15% Al as Alumina, < 200 ppm Boron, bal. Cu	Annealed
CuCr	3A	3.5% Cr Oxide, bal. Cu	20% CW, 1/2 hr 450°C, Air Cooled
CuHf	3B	1.1% Hf Oxide, bal. Cu	20% CW, 1/2 hr 450°C, Air Cooled
ODS-1	3F	0.25% Mg, 1% Alumina, bal. Cu	40% CW
ODS-1	3H	0.25% Mg, 1% Alumina, bal. Cu	40% CW + welded
ODS-4	3M	0.5% Mg, 1% Alumina, bal. Cu	40% CW

(a) All heat treatments in argon.
(b) CW = cold worked.

TABLE 3

Grain Size in Plane of Rolling Direction

Material	Material Code	Average Grain Diameter (microns)	Approximate ASTM Grain Size
Marz Cu	(RO)	120	3
CuAl25	(R4)	elongated 0.6 x 2.4	NM[a]
CuAl25 welded	(3N)	elongated 0.6 x 2.4	NM
CuAl20	(UX)	elongated 0.45 x 3.0	NM
CuAl15+B	(VO)	elongated 0.5 x 3.0	NM
CuCr	(3A)	1.0 - 11.5[b]	NM
CuHf	(3B)	1.0 - 11.5[b]	NM
ODS-1	(3F)	210	2
ODS-1 welded	(3H)	210	2
ODS-4	(3M)	100	1

(a) Not meaningful.
(b) Exhibited highly deformed, randomly shaped grains that could not be adequately characterized. Approximate size 1.0 to 11.5 microns.

TABLE 4

Average Tensile Properties from Copper and Copper Alloy Miniature Specimens

Material Code	Alloy	Yield (0.2% offset) Strength MPa (ksi)	Ultimate Tensile Strength MPa (ksi)	Fracture Strength MPa (ksi)	Uniform Elongation (%)	Total Elongation (%)	Number of Specimens
RO	Marz Cu						
	Unirradiated	74.7 (10.8)	170.6 (24.7)	4.5 (0.6)	23.2	29.0	2
	Aged 420°C, 1026 hrs.	70.5 (10.2)	170.6 (24.7)	2.1 (0.3)	16.7	20.8	2
	Irr. 34 dpa, 414°C	64.0 (9.3)	116.1 (16.8)	103.4 (15.0)	9.7	10.1	1
	Irr. 50 dpa, 411°C	63.0 (9.1)	131.2 (19.0)	119.7 (17.4)	14.7	15.0	2
VO	CuAl15						
	Unirradiated	274.4 (39.8)	359.3 (52.1)	266.2 (38.6)	12.4	15.5	3
	Aged 420°C, 1026 hrs.	301.7 (43.8)	391.4 (56.8)	306.3 (44.4)	13.4	18.3	2
	Irr. 34 dpa, 414°C	295.1 (42.8)	372.1 (54.0)	302.6 (43.9)	12.1	15.3	2
UX	CuAl20						
	Unirradiated	475.2 (68.9)	499.8 (72.5)	405.1 (58.8)	1.3	3.6	7
	Aged 420°C, 1026 hrs.	422.7 (61.3)	444.7 (64.5)	387.1 (56.1)	3.5	5.9	2
	Aged 521°C, 1026 hrs.	392.9 (57.0)	425.9 (61.8)	356.8 (51.8)	5.6	8.3	2
	Irr. 34 dpa, 414°C	377.5 (54.7)	411.3 (59.6)	345.6 (50.1)	7.9	9.9	2
	Irr. 50 dpa, 411°C	376.1 (54.5)	396.5 (57.5)	353.4 (51.2)	11.1	14.1	2
	Irr. 32 dpa, 529°C	388.4 (56.3)	440.9 (63.9)	378.4 (54.9)	10.6	14.7	2
R4	CuAl25						
	Unirradiated	501.0 (72.7)	556.1 (80.7)	462.7 (67.1)	1.5	4.3	4
	Aged 420°C, 1026 hrs.	472.7 (68.6)	501.6 (72.8)	425.4 (61.7)	4.3	8.4	2
	Irr. 50 dpa 411°C	461.2 (66.9)	481.0 (69.8)	414.2 (60.1)	8.3	11.5	2
3N	CuAl25 Laser Welded						
	Unirradiated	145.0 (21.0)	203.8 (29.6)	14.6 (2.1)	8.6	13.6	3
	Aged 420°C, 1026 hrs.	70.8 (10.3)	202.1 (29.3)	95.0 (13.8)	27.4	30.9	2
	Irr. 50 dpa, 411°C	72.9 (10.6)	142.9 (20.7)	139.7 (20.3)	13.0	13.1	2
3A	CuCr						
	Unirradiated	158.8 (23.0)	299.7 (43.5)	219.9 (31.9)	22.0	30.7	2
	Aged 420°C, 1026 hrs.	148.9 (21.6)	294.9 (42.8)	202.8 (29.4)	22.6	33.0	2
	Irr. 50 dpa, 411°C	163.0 (23.6)	308.0 (44.7)	295.1 (42.8)	18.8	19.8	2
3B	CuHf						
	Unirradiated	378.1 (54.8)	461.6 (66.9)	317.0 (46.0)	4.2	8.7	3
	Aged 420°C, 1026 hrs.	154.0 (22.3)	310.0 (45.0)	204.9 (29.7)	20.9	25.6	2
	Irr. 50 dpa, 411°C	(upper)326.8 (47.4) (lower)305.4 (44.3)	320.5 (46.5)	251.1 (36.4)	16.3	20.5	2
3F	ODS-1						
	Unirradiated	312.0 (45.3)	344.6 (50.0)	177.9 (25.8)	0.8	3.7	2
	Aged 420°C, 1026 hrs.	62.2 (9.0)	218.1 (31.6)	75.7 (11.0)	33.8	39.8	2
	Irr. 50 dpa, 411°C	87.0 (12.6)	151.5 (22.0)	92.1 (13.4)	8.4	9.3	2
3H	ODS-1 Laser Welded						
	Unirradiated	190.6 (27.6)	228.9 (33.2)	132.9 (19.3)	1.5	3.5	3
	Aged 420°C, 1026 hrs.	143.5 (20.8)	224.4 (32.5)	77.5 (11.2)	2.3	4.7	2
	Irr. 50 dpa, 411°C	123.3 (17.9)	125.9 (18.3)	119.4 (17.3)	0.4	0.4	2
3M	ODS-4						
	Unirradiated	278.3 (40.4)	352.6 (51.1)	214.8 (31.2)	0.8	3.8	2
	Aged 420°C, 1026 hrs.	55.2 (8.0)	227.1 (32.9)	150.6 (21.8)	37.1	40.9	2
	Irr. 50 dpa, 411°C	79.5 (11.5)	162.9 (23.6)	45.1 (6.5)	13.3	14.5	2

LIST OF FIGURES

1. Tensile properties of the oxide-dispersed alloys compared with zone-refined marz copper.

2. Swelling levels as measured by immersion density.

3. Swelling in copper-alumina alloys irradiated at 411 to 414°C as a function of dose.

4. Swelling in copper-alumina alloys irradiated to 50 dpa at 411°C as a function of alumina volume fraction.

5. TEM micrographs of CuAl15, (a) unirradiated and (b and c) irradiated to 50 dpa at 411°C. Total recrystallization following irradiation is evident in (b), and the development of damage structure in areas of low dispersion density is seen in (c).

6. SEM fractographs of tensile failure surfaces for the CuAl alloys, (a,c,e) unirradiated and (b,d,f) irradiated. CuAl15 (a,b) was irradiated to 34 dpa at 414°C (b); CuAl20 (c,d) was irradiated to 50 dpa at 411°C (d); and CuAl25 (e,f) was irradiated to 50 dpa at 411°C (f).

7. Large alumina particles in CuAl15, (a) unirradiated and (b) irradiated to 50 dpa at 411°C.

8. SEM fractographs of CuCr tensile fracture surfaces, (a,b) unirradiated and (c,d) irradiated to 50 dpa at 411°C. The influence of large inclusions on the fracture morphology can be noted.

9. TEM micrographs of CuCr, (a) unirradiated and (b,c) irradiated to 50 dpa at 411°C. The irradiated material is shown in a bright field (b) and dark field (c) pair.

10. TEM micrographs of CuHf irradiated to 50 dpa at 411°C. A bright field (a) and dark field (b) pair is shown where two distinct particle distributions can be seen.

11. SEM fractographs of tensile fracture surfaces of CuHf, (a,b) unirradiated and (c,d) irradiated to 50 dpa at 411°C.

12. Tensile curves of CuHf in the unirradiated, thermally aged, and irradiated to 50 dpa at 411°C conditions. The upper and lower yield phenomenon in the irradiated condition is notable.

13. SEM fractographs of the tensile fracture surfaces of the ODS-1 alloy, (a,b) unirradiated and (c,d) irradiated to 50 dpa at 411°C. The strong influence of the void structure on the tensile fracture behavior is clearly evident in the irradiated material.

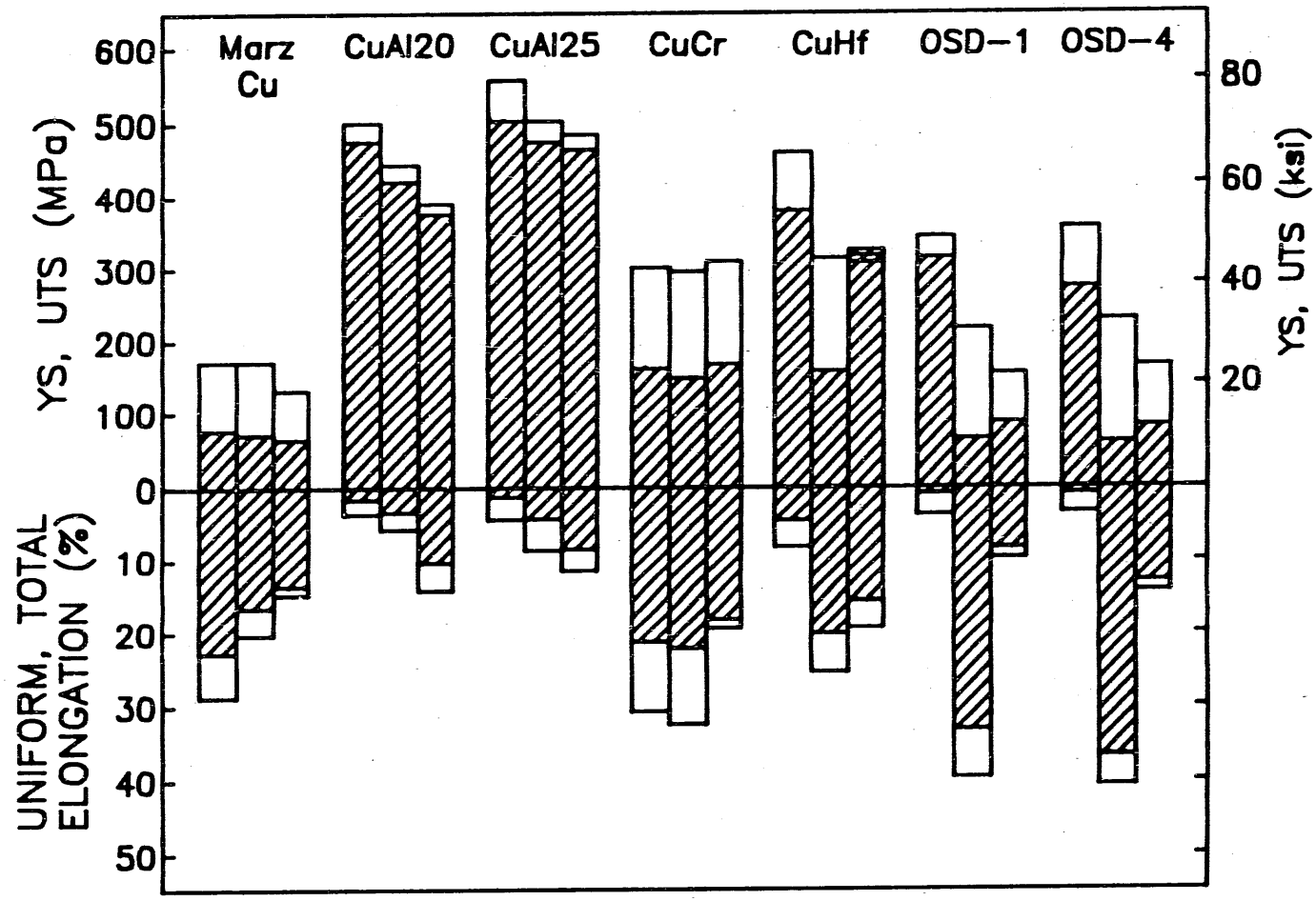
Marz Cu
CuAl20
CuAl25
CuCr
CuHf
OSD−1
OSD−4
YS, UTS (MPa)
600
500
400
300
200
100
0
UNIFORM, TOTAL ELONGATION (%)
10
20
30
40
50
YS, UTS (ksi)
80
60
40
20

Fig. 1

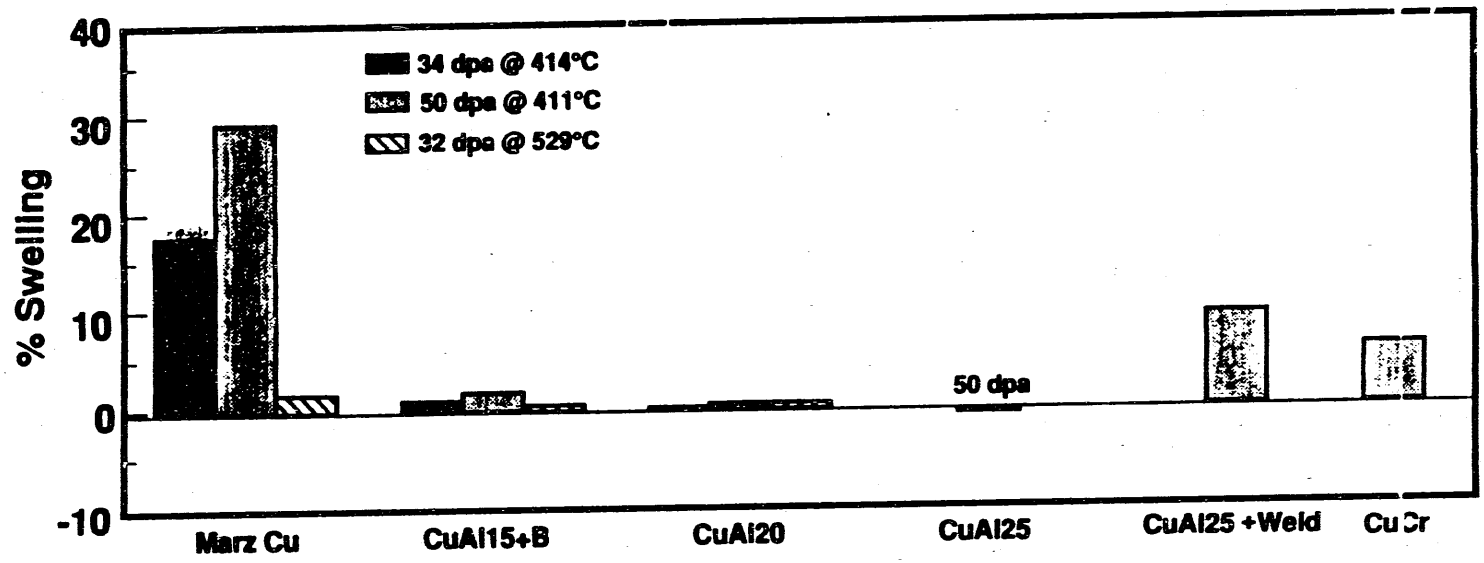

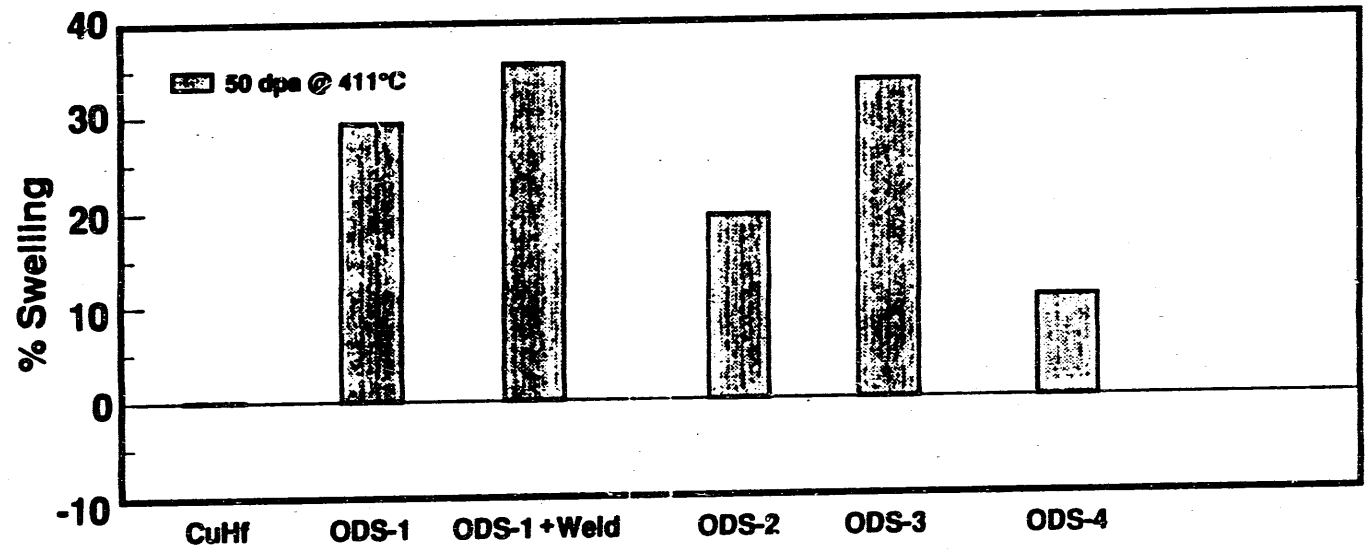

39005037.3

Fig. 2

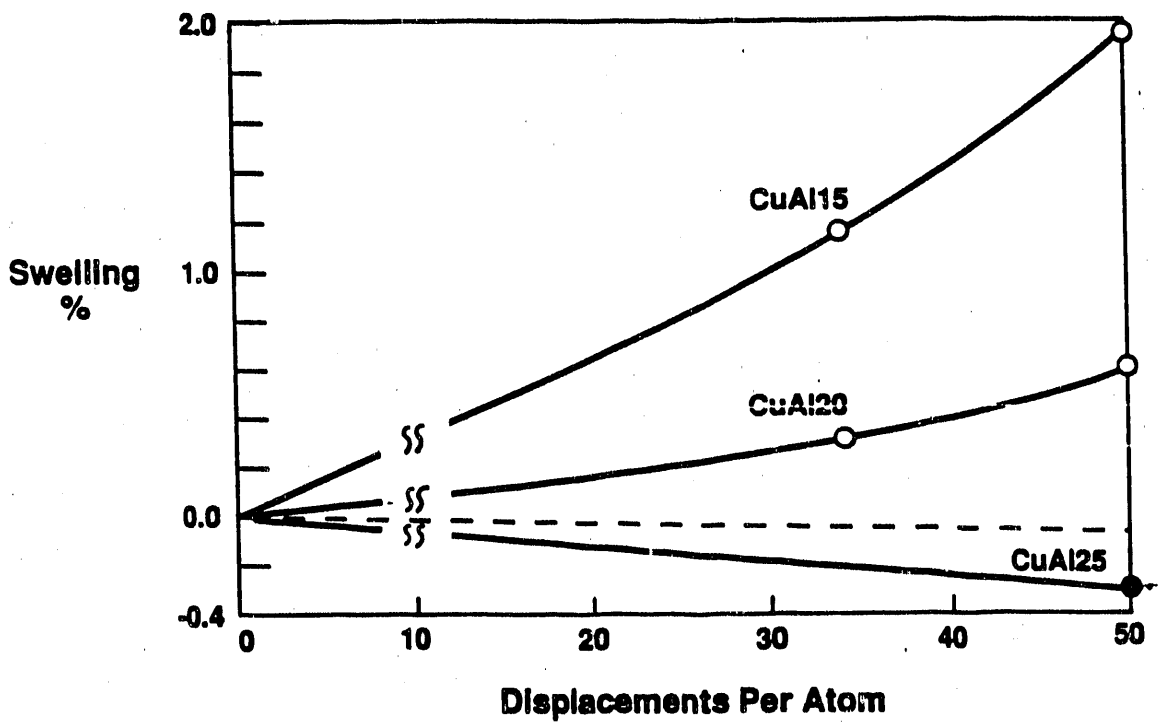
2.0
1.0
0.0
-0.4
Swelling
%
CuAl15
CuAl20
CuAl25
0
10
20
30
40
50
Displacements Per Atom

Fig. 3

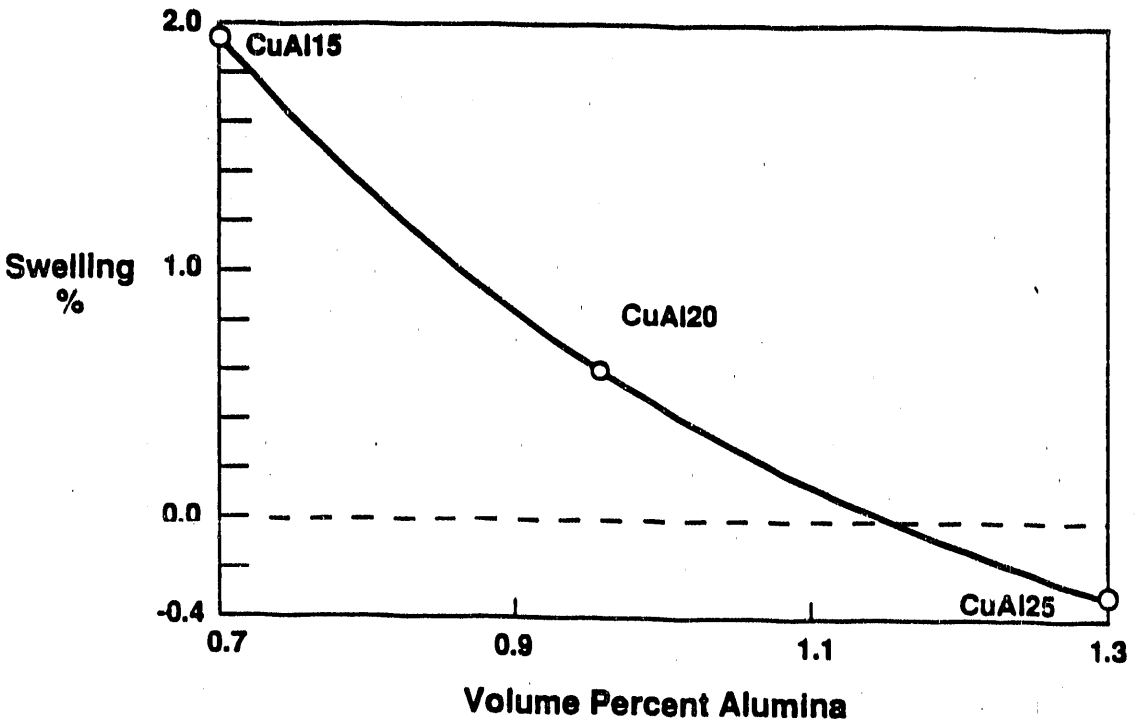
2.0
1.0
0.0
-0.4
Swelling %
CuAl15
CuAl20
CuAl25
0.7
0.9
1.1
1.3
Volume Percent Alumina

Fig 9

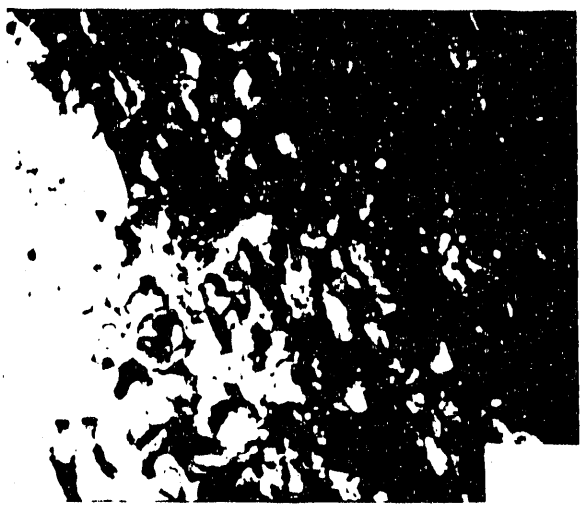

A

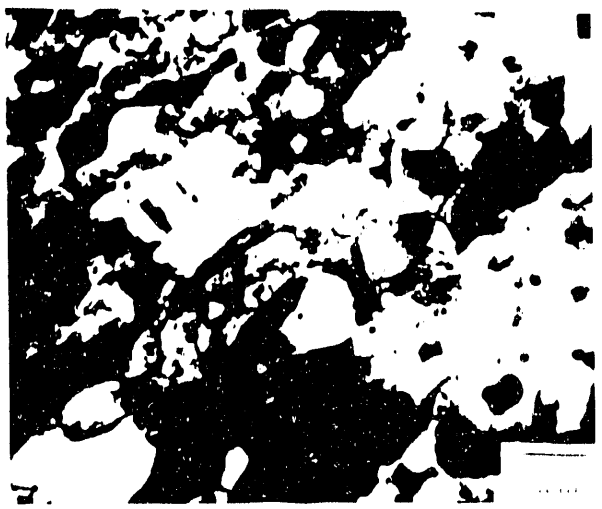

B

15KU X4000 9409 1.0U PNL

A

B

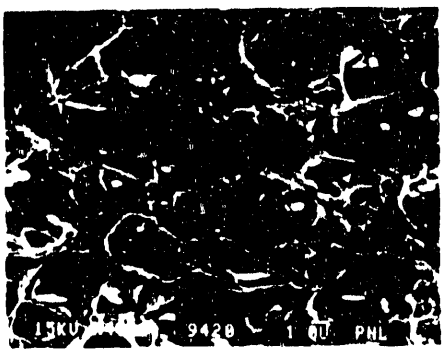
9420 1.0U PNL

C

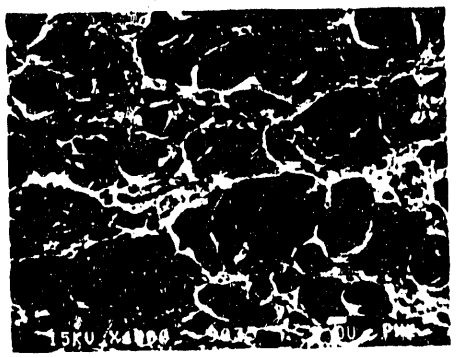

D

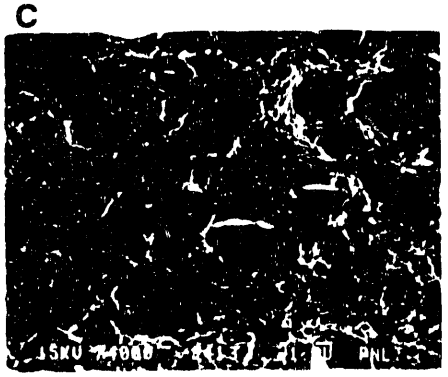
15KU X4000 PNL

E

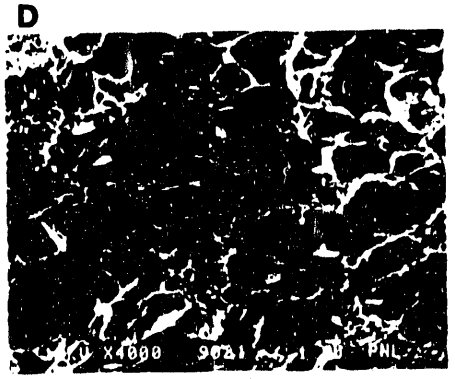
X4000 9421 PNL

F

A

B

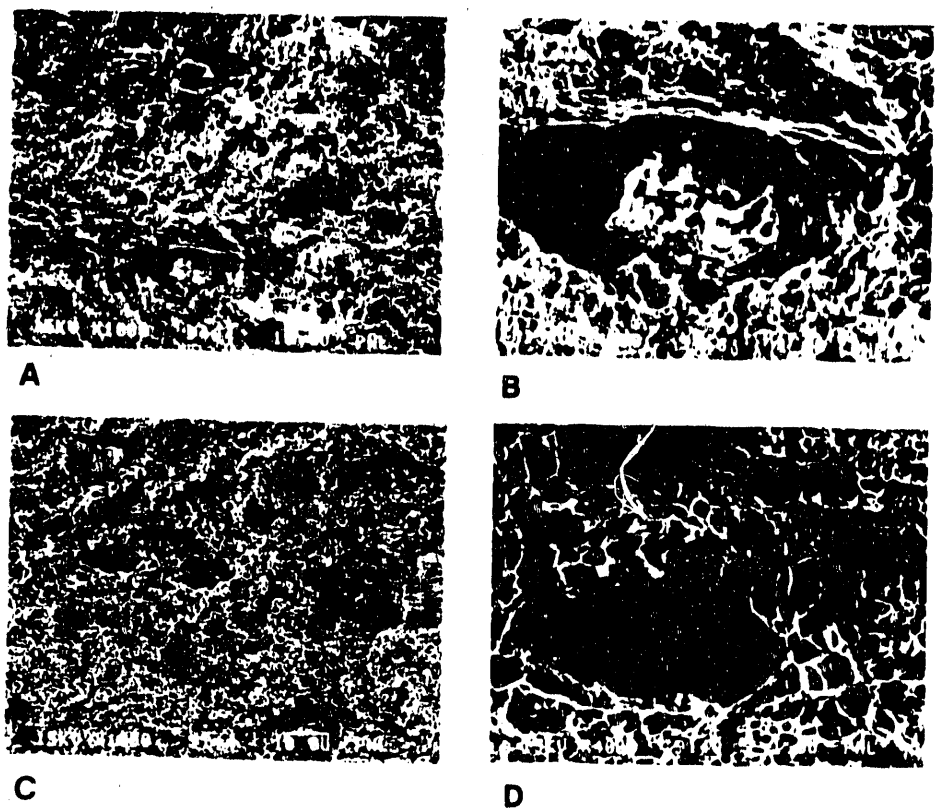
A
B
C
D

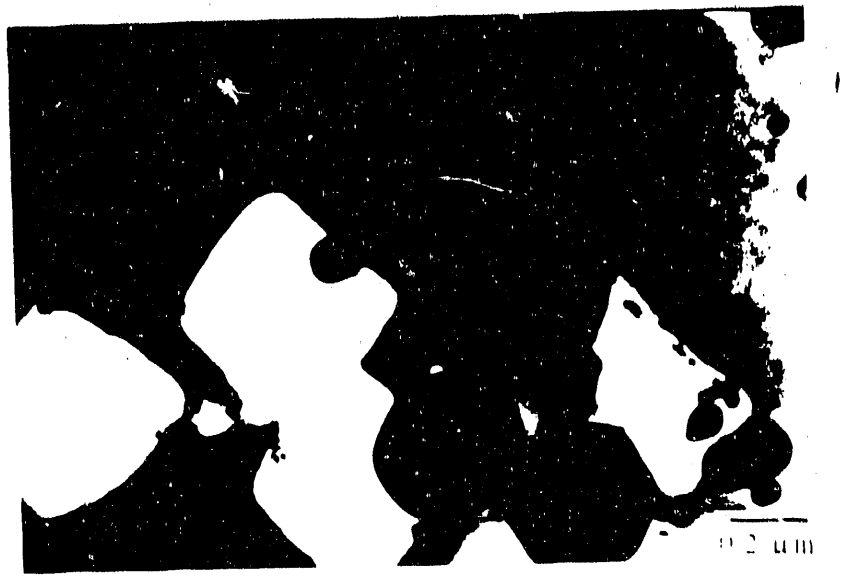

A

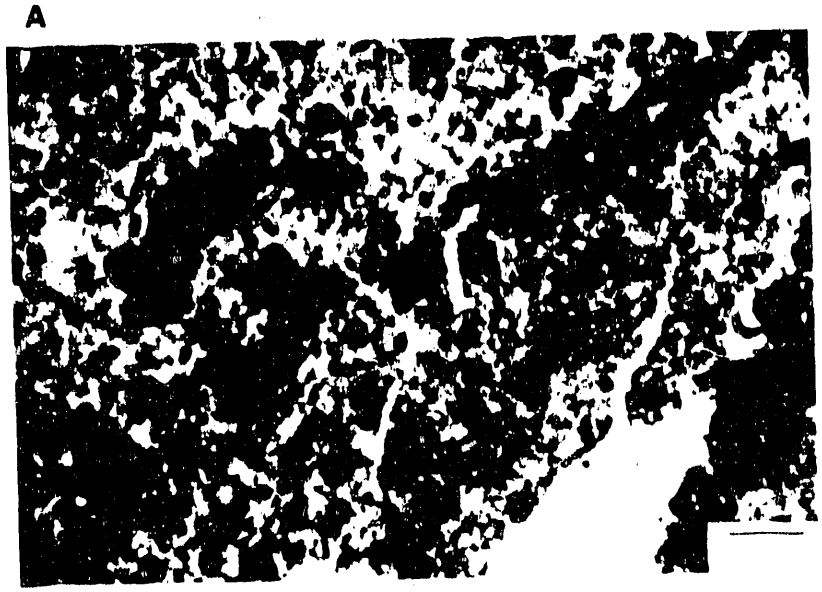

B

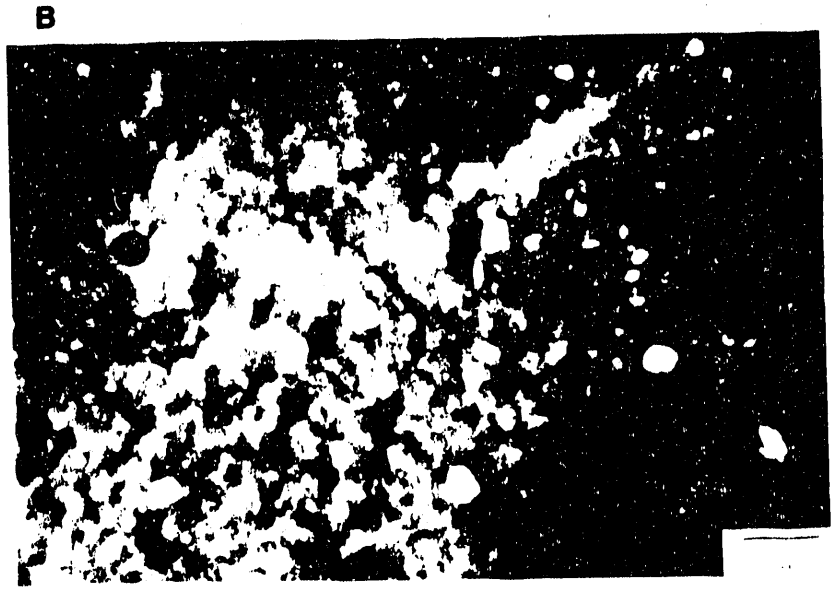

C

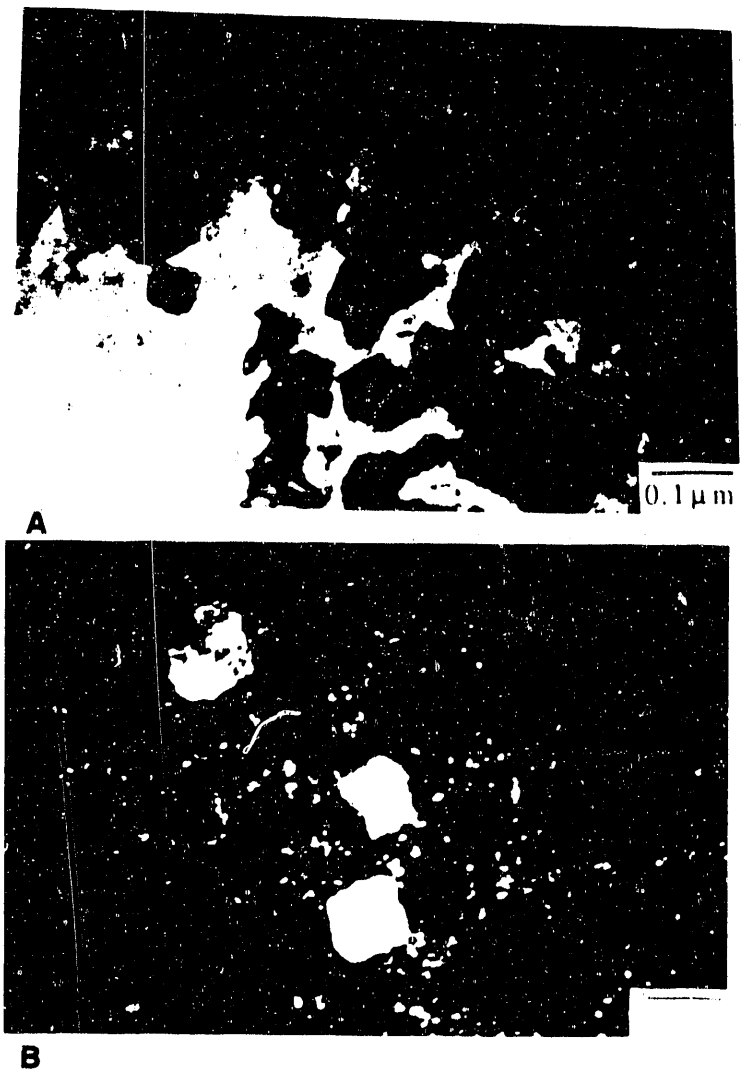
0.1 μm
A
B

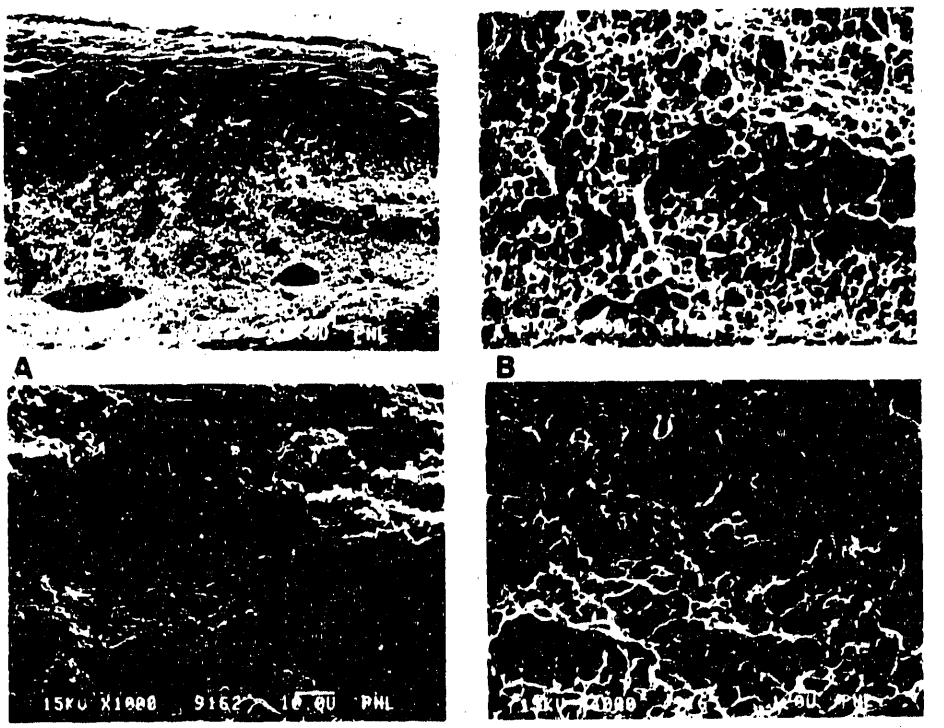
A
B
15KV X1000 9162 10.0U PNL
C
D

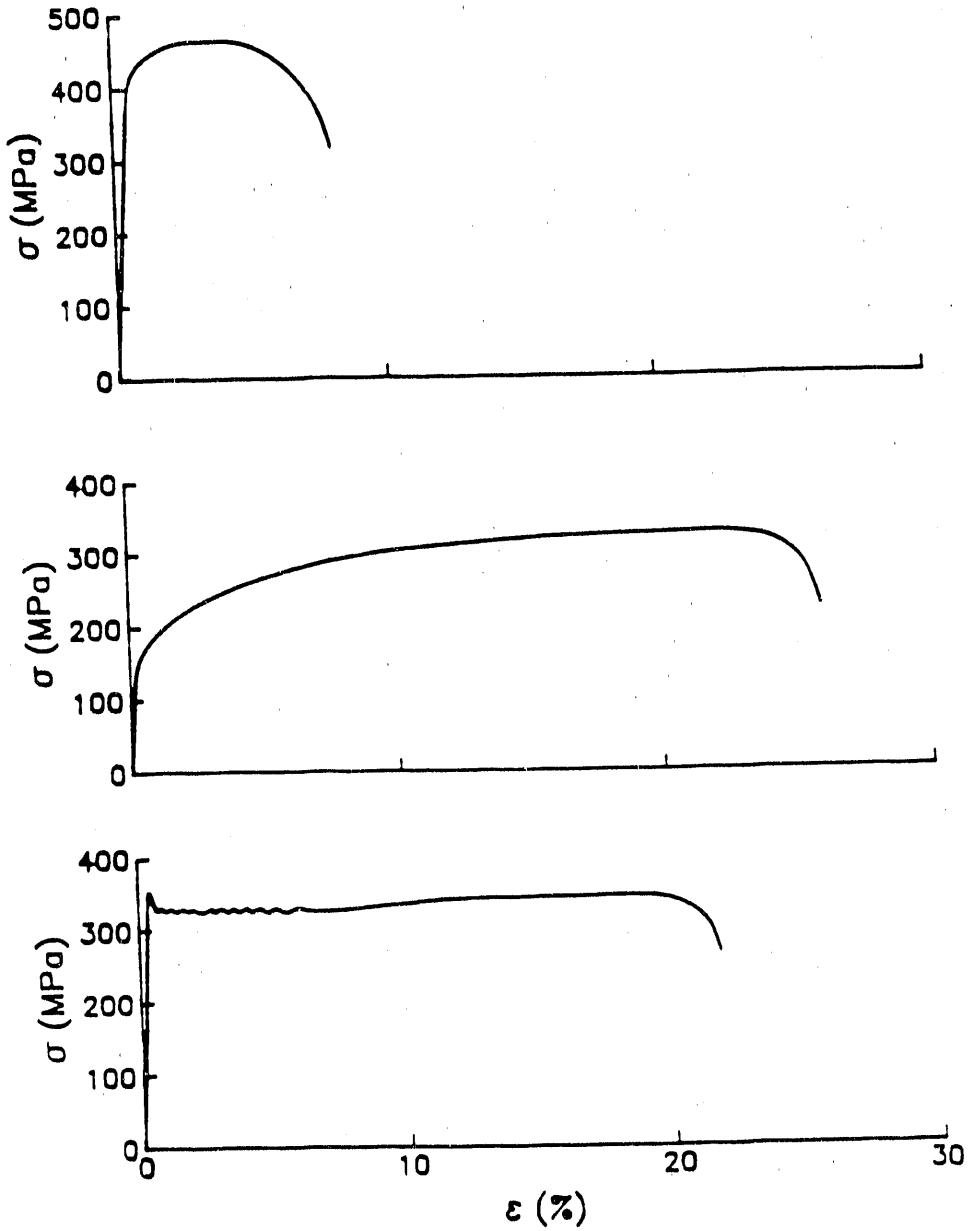
500
400
300
200
100
0
σ (MPa)
400
300
200
100
0
σ (MPa)
400
300
200
100
0
σ (MPa)
0
10
20
30
ε (%)

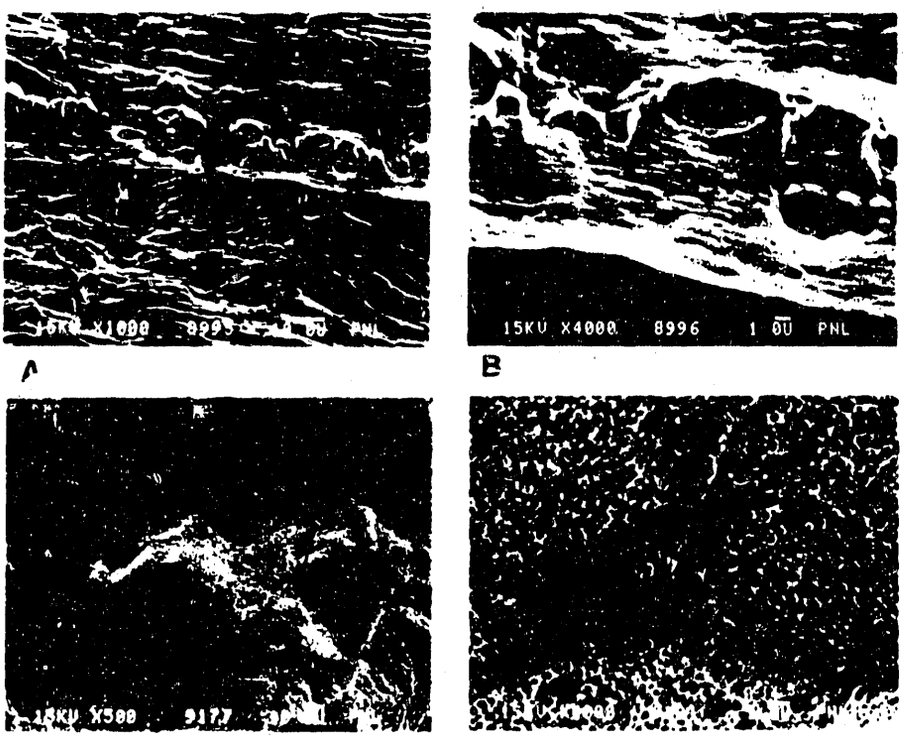
15KU X4000 8996 1 0U PNL
A
B
C
D

END

DATE FILMED

01 / 10 / 91